Journal Pre-proofs

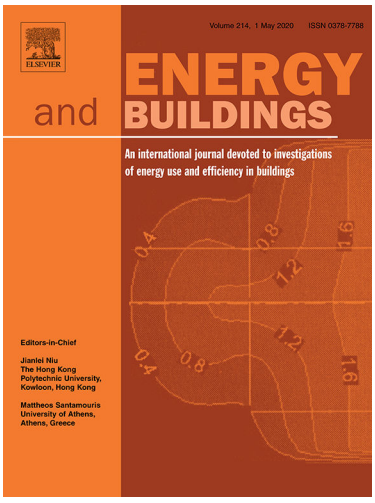

Modeling method of an active-passive ventilation wall with latent heat storage for evaluating its thermal properties in the solar greenhouse

Fengtao Han, Chao Chen, Qingling Hu, Yipeng He, Shen Wei, Caiyun Li

PII: S0378-7788(21)00124-9
DOI: https://doi.org/10.1016/j.enbuild.2021.110840
Reference: ENB 110840

To appear in: *Energy & Buildings*

Received Date: 28 October 2020
Revised Date: 1 February 2021
Accepted Date: 14 February 2021

Please cite this article as: F. Han, C. Chen, Q. Hu, Y. He, S. Wei, C. Li, Modeling method of an active-passive ventilation wall with latent heat storage for evaluating its thermal properties in the solar greenhouse, *Energy & Buildings* (2021), doi: https://doi.org/10.1016/j.enbuild.2021.110840

Highlights：

- APVW-L's model was validated against measured data with a high accuracy;
- The model was used to define the rational parameters of the proposed wall;
- A full-scale greenhouse with the proposed wall was built and tested in Beijing;
- The proposed wall can store 5.36 MJ/(m^2·day) of solar energy on a sunny day;
- The proposed wall increased indoor air temperature by 0.8~1.4 ℃ after midnight.

Modeling method of an active-passive ventilation wall with latent heat storage for evaluating its thermal properties in the solar greenhouse

Fengtao Han[1], Chao Chen[1]*, Qingling Hu[1], Yipeng He[1], Shen Wei[2], Caiyun Li[1]

1. *College of Architecture and Civil Engineering, Beijing University of Technology, Beijing 100124, P R China*
2. *The Bartlett School of Construction and Project Management, University College London (UCL), 1-19 Torrington Place, London WC1E 7HB, United Kingdom*

Abstract

Active-passive phase change heat storage technologies have been obtained extensive application to decrease greenhouse's demands for fossil energy during off-seasons. To develop the utilization ratio of solar energy in solar greenhouses during winter, the active-passive ventilation wall with latent heat storage (APVW-L) was introduced and could be integrated into greenhouse's back-wall. However, system design and operation parameters are subjected to numerous factors, including its structure, material performance and outdoor meteorological parameters. To achieve optimization in the energy performance of this system, this study used finite element analysis and lumped parameter analysis to establish coupled energy balance equations of the APVW-L and the air inside vertical air passages, and the cubic spline interpolation was used to calculate the continuous relationship between phase change material's equivalent specific heat capacity and temperature. This modeling method of the APVW-L was accurately validated against the measured data, and then used in the optimization design and operation strategy of the APVW-L in the greenhouses. This study demonstrated that the optimized APVW-L could store 5.36 MJ/(m^2·day) of solar energy in Beijing. Compared to the identical conventional greenhouses, after midnight, the experimental greenhouse having APVW-L increased the back-wall's interior surface temperature by 2.2~3.4 °C, and the average indoor air temperature by 0.8~1.4

°C. This study provides methods for the APVW-L's optimization design and its operation strategy, even for the rationalization of the near-zero energy consumption of the solar greenhouse during winter.

Keywords: solar greenhouse; active-passive ventilation wall; latent heat storage; thermal performance; mathematical model; engineering application

1. Introduction

Solar greenhouses passively utilize solar energy as their main heating source, and their application range for producing overwintering crops keeps expanding in the cold regions of northern China [1]. Although solar energy is abundant during the day, solar greenhouses' indoor air temperature often drops below the biological zero of thermophilic crops after midnight, especially during December and January. So, auxiliary heating methods such as coal furnaces, electric air heaters, and heat pumps, are used to provide additional heating [2–3].

Many existing studies have shown the importance of the back-wall's thermal properties in the greenhouse for the maintenance of interior thermal environment and reduction of heating load [4-5]. Researches have proved that phase change materials (PCMs) used in the back-wall were efficient in improving interior thermal environment [6-7]. Whereas, because of heat storage materials' unfavorable thermal conductivity, the depth of heat penetration into the back-wall via heat conduction is restricted, leading to inadequate heat storage ability during daytime [8-9]. Fang H., et al. [10] developed a water curtain system on the back-wall's interior surface to absorb solar energy, and used a water tank to storage the hot-water during daytime. At night, this system using the water circulated from the water tank could increase the indoor temperature by 5.4 °C, and the crops' rhizosphere temperature by 1.6 °C. However, this system requires a water tank having good heat retention properties and must occupy greenhouse's limited space. And the freezing and leakage of water pipelines are common problems seen during winter. In some civil buildings, some solar heating systems integrated into building envelopes are used to reduce heating load, which are worth mentioning [11-13]. Hassanain, et al.[14] developed a Trombe wall for the solar greenhouse in Suez, Egy. The research showed with indoor air temperature as 21.4 ℃, the wall's maximum interior surface temperature might approach 52 ℃, while the maximum temperature at 0.06 m away from the interior wall surface would be 38 ℃. Bao Encai, et al. [15-16] developed an active heat storage wall comprising porous bricks with solidified sands. They found that the wall's heat storage capacity was 2.44~3.58 MJ/m^2, and its heat release capacity was 1.12~1.2 MJ/m^2 on a sunny day. Guan Yong, et al.[9] developed an active-passive heat storage wall with built-in tanks filled with PCM. However, improving the solar absorption capacity of the back-wall's internal surface by using PCMs is more effective to reduce heating load [17-19].

For improving the utilization ratio of solar energy in winter, an active-passive ventilation wall with latent heat storage (abbreviated as APVW-L) was proposed [7]. This wall with a solar air collector system could be integrated into the solar greenhouse's back-wall to decrease heating load. Thus the design and operation parameters of this system are subjected to numerous factors, including its structure,

material performance and outdoor meteorological parameters. However, due to the complex and changeable outdoor meteorological conditions, it is difficult to determine these parameters one by one through experiments. Therefore, numerical analysis is required to solve these problems and even to provide methods for the optimization design and operation strategy of the APVW-L in the solar greenhouse.

Chao, et al. [20] employed EnergyPlus in optimizing solar greenhouse's physical dimensions to gain more solar energy and reduce heating load in winter. Roman et al. [21] simulated PCM roof's dynamic thermal performance with DesignBuilder and EnergyPlus, achieving a reduction of 54% heat demands by using PCM roof. Ma et al. [22] considered THERB for HAM, a dynamic thermal load computing tool developed by A. Ozaki, to be suitable for optimizing the energy properties of a composite Trombe wall in an office building. And this research showed that this wall with optimized ventilation could decrease energy costs by 3.7% annually at most. Nguyen et al. [23] proposed one solar chimney having a horizontal absorber surface. This solar chimney could be integrated into building envelopes for natural ventilation or energy conservation. However, this research only investigated how heat flux and chimney dimension influenced air flow rate and thermal efficiency with CFD software. Tong Guohong [24] used CFD software to analyze the variation of temperature field with the thickness of the composite walls applied onto solar greenhouses. The results revealed that when wall thickness was 0.60 m, the thicker the heat storage layer was, the faster the internal temperature decayed. And the determination of heat storage layer's thickness was related to where insulation layer located in the composite wall. Bao Encai, et al.[25] set up air passages inside the greenhouse's back-wall for active heat storage, and used CFD software to analyze how various airflow directions influence this wall's active heat storage, to optimize the air distribution, and the positions of air inlet and outlet. Jovanovic, et al. [26] used system advisor model software to study the energy-efficiency and electricity inside a building produced by the Trombe wall and PV modules. Lin et al. [27-28] designed a Trombe wall having PV panels in wall's passage, and developed a mathematical model for this system to study its thermal performance. The results showed that this system had 65.2% higher thermal efficiency than the classic Trombe system. Zhang X. et al. [29] used CFD to develop a solar greenhouse model, and numerically analyzed how back-wall's thickness affected interior air temperature. In the previous studies, these models could not easily reflect the coupling effect of the heating system and outdoor meteorological parameters, and lacked dynamic verification under the changes in multiple factors in the application process.

Also, PCMs' thermophysical properties, especially the specific heat capacity, vary significantly with temperature. These properties are tested experimentally [30-31]. But discontinuous test values cannot be input in the numerical model. Generally, fitting formulas and numerical approximation are often used as PCM's specific heat capacity to put into the model's calculation [32-33]. For example, Haoshu Ling [32] introduced three different and common methods proposed in many studies, including 1) simplifying PCMs' specific heat capacity of charging or discharging as one value, 2) supposing PCMs' specific heat capacity of charging or discharging exhibited linear

changes with temperatures, and 3) estimating the numerical approximation of temperature step as 0.01 °C. He then used these methods respectively in his mathematical model to calculate the internal surface temperature of the active-passive ventilation wall with latent heat storage, and obtained average temperature errors were 1.96 °C, 1.74 °C and 1.31 °C, with the maximum temperature errors of 4.76 °C, 3.44°C and 2.81 °C, respectively. However, this model did not examine changed air temperature's coupling effect inside vertical air passages on the temperature field inside the wall, and did not effectively verify the calculation of temperature field of this wall, including the air temperature inside the vertical passage.

According to the structural characteristics and working principle of the APVW-L, energy conservation theory was taken for its heat transfer analysis. To optimize the system energy properties, this study used finite element analysis and the lumped parameter analysis to establish coupled energy balance equations of the APVW-L and the air inside vertical air passages, and the cubic spline interpolation was used to calculate the continuous relationship between PCM's equivalent specific heat capacity and temperature. This modeling method of the APVW-L was validated against the measured data, then used to study the influence of the multi-factor coupling on the thermal performance of the APVW-L, and its reasonable parameters were provided. Moreover, an experimental solar greenhouse having this system was built in Beijing and compared with a conventional greenhouse to show the practical effects of APVW-L. This study provides methods for APVW-L's optimization design and its operation strategy, even for the rationalization of the near-zero energy consumption of the solar greenhouse during winter.

List of abbreviations

APVW-L Active-passive ventilation wall with latent heat storage

B Dimension of air passage along Y-axis, m

c_p Specific heat capacity, kJ/(kg·°C)

f Frictional coefficient

H The enthalpy of PCM layer in a certain temperature region, J/(kg·K)

h_{air} Convective heat transfer coefficient between air and interior surface of vertical air passage, W/(m²·K)

H The enthalpy of PCM layer

t_f Air temperature on wall surface, °C

t_i Time, s

t_n The maximum temperature in the whole test interval of DSC curve, °C

t_w Wall surface temperature, °C

T Measured values of air temperature, °C

v_f Wind speed in the environment, m/s

v_0 Air velocity, m/s

V Volume, m³

Subscript

a air

$_{max}$	after complete phase transformation, J/(kg ·K)
h_q	Convective heat transfer coefficient between wall surface and air, W/(m^2·K)
I	Solar radiation intensity on wall surface, W/m^2
I_A	Index of agreement
k_s	Absolute roughness, mm
L	Dimension of air passage along X-axis, m
MSC-DRTs	Multi-surface solar air collector with double-receiver tubes
$NMBE$	Normalized mean bias error, %
$RMSE$	Root mean square error, %
Pr	Prandtl criterion number
Q_f	Convective heat transfer on the wall surface, J
Q_x	Heat storage capacity of the cement block/brick layer and insulation layer, J
Q_q	Total heat storage of PCM layer, J
R	Hydraulic radius of air passage, m
S	Area of wall surface, m^2
St	Stanton criterion number
t	Temperature, ° C
t_1	The minimum temperature in the whole test, ° C
t_n	The maximum temperature in the whole test, ° C
t_b	Phase change onset temperature, ° C
$_{ir}$	
$_{back}$	Interior surface of the vertical air passage away from indoor
$_{front}$	Interior surface of the vertical air passage near indoor
$_{in}$	Indoor
$_{out}$	Outdoor
$_{right}$	Right/left interior surface of the vertical air passage
t_{i_0}	Initial time
x	Coordinate node along the X-axis
y	Coordinate node along the Y-axis
z	Coordinate node along the Z-axis

Greek letters

α	Absorptivity of interior surface of the APVW-L
η	Phase change rate of PCM layer, %
η_i	i^{th} measured value
η_{pave}	Average of measured values
λ	Thermal conductivity, W/(m·K)
ρ	Density, kg/m^3
χ_i	The i^{th} simulate value
χ_{pave}	Average of simulation values
$\angle_x$	Step length along X-axis, m
$\angle_y$	Step length along Y-axis, m

t_e	Phase change offset temperature, °C	$\angle z$	Step length along Z-axis, m

2. Design concept of the APVW-L integrated into the solar greenhouse

For promoting the utilization ratio of solar energy and reducing the heating load in the solar greenhouse during winter, an APVW-L equipped with solar air collectors (MSC-DRTs [34]) is presented for integration into the greenhouse's back-wall (Fig 1). The APVW-L uses polyphenyl insulation board (3) as the insulation layer on its exterior surface and uses the aforementioned GH-20 composite phase change wallboard (1) as the PCM layer on its interior surface. The equivalent specific heat capacity of GH-20 composite phase change wallboard is presented in Fig. 2, and its heat of fusion is 75 kJ/kg [32]. The middle layer of the APVW-L is a cement block/brick wall (2), and its interior having vertical air passages (4) to receive hot airflow. Table 1 shows the APVW-L's materials and their thermal property parameters.

1 - GH-20 composite phase change wallboard; 2 - Cement block/brick wall; 3 - Polyphenyl insulation board; 4 - Vertical air passage

Fig. 1 APVW-L integrated into solar greenhouse's back-wall

Table 1 Thermal property parameters of APVW-L's materials

Materials	Density, kg/m^3	Specific heat capacity, J/(kg·℃)	Thermal conductivity, W/(m·℃)	Heat storage coefficient, W/(m·℃)	Absorptivity
GH-20 composite phase change wallboard	900	**Fig. 2**	0.4	16.14 [35]	0.75
Cement block/bricks	1800	1050	0.81	10.54	0.7
Polyphenyl insulation board	30	1380	0.042	0.36	—

Fig. 2 GH-20 composite phase change wallboard's equivalent specific heat capacity

For such a system in the solar greenhouse, APVW-L's interior surface passively absorbs solar energy penetrating across the solar greenhouse's front-roof, and middle layer can be heated by hot air from solar air collectors during daytime. The solar energy can be stored in the APVW-L using the above two ways simultaneously, and the accumulated energy in the APVW-L can be released into indoor environment at night via heat radiation and convection. Because of the complex and changeable meteorological conditions, it is difficult to analyze how multi-factor coupling affects APVW-L's thermal performance, and even more difficult to determine the optimal structure and operation parameters of the APVW-L one by one through experiments. Therefore, numerical analyses are needed to solve these problems.

3. Modeling method of the APVW-L

3.1 Modeling scheme and assumptions

Fig. 3 shows the APVW-L's sectional view and its heat transfer process. According to the structural characteristics and working principle of this wall (as described in Section 2), the following assumptions are made:

(a) Side view (B-B section) **(b) View from the top (A-A section)**

1 - GH-20 composite phase change wallboard; 2 - Cement block/brick wall; 3 - Vertical air passage; 4 - Polyphenyl insulation board; 5 - Vertical air passage filled with sand and stone;

Fig. 3 Sectional view of the APVW-L

- The air temperature on the same section of the vertical air passage is uniform, and the air velocity along the height of the vertical air passage remains the same.
- The boundary conditions at the top and bottom of the APVW-L are supposedly adiabatic.
- The central axis of the air passage is taken as the boundary (Fig. 3b), and the thermal features on the left and right sides of this central axis are axisymmetric. Thus this central axis is assumed to be an adiabatic boundary.
- As indicated by the results of the experiment [36], the thermal influencing radius of the air passage is around 250 mm. Along the length of the APVW-L, the boundary away from the air passage (more than 500 mm) is considered to be an adiabatic boundary.

According to the assumptions mentioned above, and by considering the spatial scale of the air passage inside the APVW-L to be small, the three-dimensional heat transfer process of the APVW-L is reduced to two two-dimensional heat transfer processes on the A-A section and the B-B section, further interrelating them through the three-dimensional heat transfer process of hot air inside the vertical air passage. See

Fig. 3, the finite element analysis was used to make two systems of algebraic equations, including the two-dimensional energy balance at every node on B-B section (Y-axis and Z-axis) and the two-dimensional energy balance at every node on A-A section (X-axis and Y-axis). Further, the finite element analysis and the lumped parameter analysis were used to make a system of algebraic equations of three-dimensional energy balance at each node of the air along the vertical air passage. Besides, the cubic spline interpolation was used to accurately calculate the continuous relationship between GH-20 composite phase change wallboard's equivalent specific heat capacity and temperature. Relevant code was used for the iterative computing of these equations. This calculation scheme not only shortens the calculation time by reducing the dimension of calculation, but also easily pairs with the mathematical model of the MSC-DRTs [34].

3.2 Energy balance for each node of the hot air inside the vertical air passage

See Fig. 3a, by using the finite element analysis and the lumped parameter analysis, the energy balance formula of the hot air at z^{th} node inside vertical air passage can be written as

(1)

where $h_{air,\,z}$ is the convective heat transfer coefficient on the vertical air passage's inner surface at node z^{th} [37].

(2)

here

(3)

where

(4)

where k_s is the absolute roughness of the air passage's inner surface. In this calculation, this value was assumed to be 1~3 mm, as reported in [38].

See Fig. 3a, air temperatures inside the air passage at z=1 and $z = z_1$ are the inlet and outlet air temperatures. Considering the change in the physical parameters of air with temperature, the related formulas could be fitted by using the experimental data from [37].

3.3 Energy balance for each node in different calculational area of APVW-L

(1) Energy balance for each node at different boundaries

For the APVW-L's external surface on the section B-B, see Fig. 3a, the energy balance equations for the node ($y=y_5$, $z=1$ or z_1) and the nodes ($y=y_5$, $z=2\sim z_1-1$) are respectively determined as

(5)

(6)

where h_q denotes the convective heat transfer coefficient on the APVW-L's surface, which can be computed as Eq. (7) [39]. This formula considers the integrated effects of convective and radiation heat transfers [40].

(7)

For this wall's inner surface on the section B-B, see Fig. 3a, the energy balance equations for the node ($y=1$, $z=1$ or z_1) and the nodes ($y=1$, $z=2 \sim z_1-1$) are respectively

determined as

(8)

(9)

For the wall's upper boundary and bottom boundary on the section B-B (when z=1 and z_1), as shown in Fig. 3a, the energy balance equations for the nodes (y=2~y_2-1, z=1 or z_1) and the nodes (y=y_3+1~y_5-1, z=1 or z_1) are respectively determined as

(10)

Similarly, the energy balance equations for each node at different boundaries of section A-A, as shown in Fig. 3b, can be written by analogy with Eqs. (5)~(10).

(2) Energy balance for each node at the inner surface of the vertical air passage

For the upper boundary of vertical air passage's inner surface on the section B-B, as shown in Fig. 3a, the energy balance equation for the node (y=y_2 or y_3, z=1) is determined as

(11)

For the bottom boundary of vertical air passage's inner surface on the section B-B, as shown in Fig. 3a, the energy balance equation for the node (y=y_2 or y_3, z=z_1) is determined as

(12)

When z=2~z_1-1 (y=y_2 or y=y_3), as shown in Fig. 3a, the energy balance equation for each node at vertical air passage's inner surface is determined as

(13)

On the vertical air passage's surface at the height of *z*, the energy balance equations for the node (x=1, y=y_2 or y_3), nodes (x=2~x_1-1, y=y_2 or y_3) and nodes (x=x_1, y=y_2+1~y_3-1), see Fig. 3b, are respectively determined as

(14)

(15)

(16)

(3) Energy balance for each node in the wall

See Fig. 3a, the energy balance equation for each node ((y=2~y_2-1 or y_3+1~y_5-1, z=2~z_1-1) in the wall is determined as

(17)

Similarly, the energy balance equations for the nodes [(x=2~x_2, y=2~y_2-1), (x=2~x_2, y=y_3+1~y_5-1) and (x=x_1+1~x_2-1, y=y_2~y_3)] in the wall on the section A-A, see Fig. 3b, can be written by analogy with Eq. (17).

3.4 Calculation method of PCMs' equivalent specific heat capacity

The discontinuous test values are presented in Fig. 2. The cubic spline interpolation was used for calculating the continuous relationship between the GH-20 composite phase change wallboard's equivalent specific heat capacity and temperature. Using this method, the APVW-L's mathematical model can accurately calculate the temperature field inside PCM layer. The calculation method is as follows:

As depicted in Fig. 2, for temperature t_j, there exists a sole equivalent specific heat capacity $c_p(t_j)$ corresponding to it. To establish the mapping relationship between the equivalent specific heat capacity and temperature, the test interval of temperature is divided into n-1 small intervals. For a small temperature interval [t_j, t_{j+1}] (j=1,2,3..., n-1), $c_p(t_j)$ can be approximately written as a cubic function of the temperature t_j, as follows

(18)

The second derivative of Eq. (18) is a function of the temperature t_j, and let $c_{p,j}''(t_j)=M_j$, $c_{p,j}''(t_{j+1})=M_{j+1}$, $h_j=t_{j+1}-t_j$, then,

(19)

Because the equivalent specific heat capacity continuously changes in the temperature interval, thus,

(20)

Then, A_j and B_j in Eq. (19) are respectively determined as

(21)

(22)

Therefore, Eq. (19) can be determined as

(23)

As the equivalent specific heat capacity continuously changes in the whole interval, so,

(24)

Then，

(25)

In the Eq. (25), $u_j=h_{j-1}/(h_{j-1}+h_j)$, $d_j=6/(h_{j-1}+h_j)[(c_{p,j+1}-c_{p,j})/h_j-(c_{p,j}-c_{p,j-1})/h_{j-1}]$ and $r_j=1-u_j$.

As shown in Fig. 2, in the case that real temperature of GH-20 composite phase change wallboard is below the minimum test temperature t_1 or greater than the maximum test temperature t_n, $c_p(t)$ does not change, so,

(26)

Then,

(27)

(28)

In Eqs. (27) and (28)， $d_1=6(c_p(2)-c_p(1))/h_1^2$， $d_n=6(c_p(n\text{-}1)-c_p(n))/h_{n\text{-}1}^2$。

According to Eq. (25), Eq. (27) and Eq.(28), Eq. (29) can be obtained.

(29)

Using Gaussian elimination method to solve Eq. (29), and M_j and M_{j+1} in any small temperature interval $[t_j, t_{j+1}]$ (j=1,2,3..., n-1) can be obtained. Then, Eq. (23) in any small temperature interval $[t_j, t_{j+1}]$ (j=1,2,3..., n-1) can be obtained.

Taken together, the continuous mapping relationship between the GH-20 composite phase change wallboard's equivalent specific heat capacity and temperature can be obtained.

3.5 Solving procedure

The algebraic equation set, revealing air temperature variation along the vertical air passage and its influence on APVW-L's temperature field, could be solved using MATLAB, and corresponding iterative computing algorithm is as shown in Fig. 4.

Fig. 4 Solving procedure of APVW-L's mathematical model

The input data include APVW-L's physical and operating parameters, outdoor meteorological parameters and indoor air temperature, etc. The numerical results could show APVW-L's temperature field and air temperature variation along the air passage. The solution convergence standard in this mathematical model is 0.01 ℃. The time-step value describing the changes in the observed data is 30s. The step lengths along the thickness (Y-axis) and length (X-axis) are 0.005 m, and the step length along the height (Z-axis) is 0.05 m.

3.6 Evaluation methods of the APVW-L's mathematical model

Besides using absolute error and relative error, this study also used index of agreement (*IA*) [20, 34], normalized mean bias error (*NMBE*) [41] and root mean square error (*RMSE*) [41]. For *IA*, the closer this value is to 1, the better the numerical values agreement with measured values. For the values of *NMBE* and *RMSE*, the numerical results shall have a *NMBE* of less than 10% and a *RMSE* of less than 30% relative to hourly calibration. *IA*, *NMBE* and *RMSE* can be calculated by Eqs. (30)~(32), respectively.

(30)

(31)

(32)

where η_i is the i^{th} measured value, χ_i is the i^{th} simulate value, η_{pave} is the actual mean value, χ_{pave} is the average of all calculation data.

4. Experimental validation of APVW-L's mathematical model

4.1 Experiment setup

Considering the difficulty in measuring the APVW-L's temperature field in the actual greenhouses, a laboratory experiment setup of the APVW-L (Fig. 5) is used to validate the presented mathematical model's accuracy. This experiment setup consists of the APVW-L (1.76 m long, 1.15 m high and 0.28 m thick), indoor air-conditioning system, air heater, fan, anemometer and temperature logger Agilent 34970A with some K-type thermocouples, etc..

1 - GH-20 composite phase change wallboard; 2 - Cement block/brick wall with vertical air passage; 3 - Polystyrene insulation board; 4 - Inlet of the vertical air passage; 5 - Outlet of the vertical air passage; 6 - Vertical air passage

Fig. 5 Experimental setup of the laboratory prototype and instrumentations

In Fig. 5, the GH-20 composite phase change wallboard is 40 mm thick, the polyphenyl insulation board is 50 mm thick, and the cement block/brick wall is 190 mm thick. The length, width and height of the vertical air passage are 0.13 m, 0.14 m and 1.15 m, respectively. Materials' thermal performance parameters can be consulted in Table 1 and Fig. 2.

4.2 Experimental scheme and data acquisition

During the experiments, the indoor air-conditioning system was used for maintaining indoor temperature at 23.5±0.5 ℃, and the air heater was used to produce the hot air at 60±0.5 ℃. Under the action of a small fan, the hot air was sent to the air inlet of the vertical air passage. The air velocity inside the vertical air passage was 0.26 m/s. The APVW-L's initial temperature field was consistent with the laboratory's indoor temperature.

Apart from being installed at the vertical air passage's inlet and outlet and in the surrounding environment of the APVW-L, the K-type thermocouples were installed on the horizontal section 0.575 m higher than the vertical air passage's outlet (see Fig. 6). The accuracy of K-type thermocouples was ±0.3 ℃. The air velocity in the vertical air passage was measured by using the Testo-435 hot-wire anemometer, and its accuracy was ±0.01 m/s. This test lasted for 8 hours and the sampling frequency of experimental values was 30 s.

Fig.6 Distribution of temperature measuring points on the horizontal section of the APVW-L

4.3 Error analysis of the numerical calculation

Fig. 7 shows the comparison of calculated and measured temperatures along the APVW-L's length direction (y=135 mm, z=575 mm). Fig. 8 shows the comparison of calculated and measured temperatures along the APVW-L's thickness direction (x=90 mm, z=575 mm). By these comparisons, the average relative error and maximum absolute error of this model were 2.5 % and ± 2.3 ℃, respectively. The *NMBE* and *RMSE* of this model were 0.96 % and 5.87 %, respectively. So this model can accurately simulate the APVW-L's temperature field under laboratory conditions.

(a) Measured temperatures (b) Calculated temperatures

Fig. 7 Comparison of calculated and measured temperatures along the APVW-L's length direction (y=135 mm, z=575 mm)

(a) Measured temperatures (b) Calculated temperatures

Fig. 8 Comparison of calculated and measured temperatures along the APVW-L's thickness direction (x=90 mm, z=575 mm)

Using this model, the dynamic variation of the APVW-L's temperature field and the air temperature inside the vertical air passage with time can be calculated. Then, the APVW-L's heat storage capacity, GH-20 composite phase change wallboard's phase change rate, APVW-L's heat release capacity, etc. can be calculated dynamically. Using these calculation results, the optimization design and operation strategy of APVW-L in the solar greenhouse can be obtained for improving the utilization of solar energy.

5. Optimization design method of the APVW-L in the solar greenhouse

5.1 Numerical strategy for a proposed greenhouse

To provide the optimization design of APVW-L in a proposed greenhouse and measure its benefits, a conventional greenhouse in Beijing, China was selected as a reference. For this conventional greenhouse's back-wall, which was different from the proposed one, its inner surface is the cement block/brick wall and 390 mm in thickness, with no vertical air passages inside, while its outer surface is the polyphenyl insulation

board and 100 mm in thickness.

Note: Outdoor wind speeds are the average values within 30 minutes.

Fig. 9 Outdoor meteorological conditions and indoor air temperature (a sunny day)

The following numerical analysis was performed on a sunny day in winter in Beijing, and solar radiation intensity, outdoor temperature, outdoor wind speed, indoor temperature in the conventional greenhouse, see Fig. 9, were selected as the input parameters. The initial value of APVW-L's temperature field was set as the indoor temperature of 6.45 ℃ at 8:30 am, and two days' trial calculation was required before the formal calculation. Considering that the indoor environment of the greenhouse was relatively closed in winter, the indoor wind speed was low and assumed to be 0.2 m/s in the following numerical analysis.

5.2 **Calculation methods of the thermal performance parameters**

(1) Cement block/brick layer's sensible heat storage

During the daytime, the cement block/brick layer can store sensible heat from hot air. This part of heat storage capacity Q_x can be calculated by Eq. (33). Since the initial time ti_0, if Q_x increases positively, the cement block/brick layer is in the process of heat storage. Otherwise, the cement block/brick layer is in the process of heat release.

(33)

(2) GH-20 composite phase change wallboard's heat storage capacity

During the daytime, GH-20 composite phase change wallboard not only stores sensible heat, but also stores latent heat. According to Fig. 2, its total heat storage capacity Q_q can be calculated by Eq. (34).

(34)

where t_b is the phase change onset temperature, ℃, t_e is the phase change offset temperature, ℃. They depend on differential scanning calorimeter (DSC) measurement.

(3) GH-20 composite phase change wallboard's phase change rate

Phase change rate refers to the ratio of PCM's mass which experiences phase transition per unit time [41]. The larger this parameter, the greater is the degree of phase

transition.

(35)

where H and H_{max} are the GH-20 composite phase change wallboard's enthalpies in a certain temperature region and after complete phase transformation, respectively, kJ/(kg ·℃).

(4) Heat transfer of APVW-L's surface

Heat transfer of APVW-L's surface can show the heating capacity of APVW-L to the solar greenhouse, and the heat insulation ability of its outer layer, which is determined as follows:

(36)

where h_q can be calculated by Eq. (7) [38-39], which considers the combined impacts from convective heat transfer and radiation heat transfer [39].

5.3 Numerical analysis and optimization

5.3.1 Variation in the APVW-L's temperature field on a sunny day

Fig.10 presents the variation in the APVW-L's temperature field in a sunny day. During the daytime (8:30 to 16:30), the APVW-L accumulates heat by passively absorbing solar energy and actively storing heat from hot air. The APVW-L's heat storage capacity reaches the maximum value at 16:30. At night (16:30 until 8:30 of the next day), the APVW-L emits heat. As shown in Fig. 10b, the heat from hot air and solar radiation have little effect on the place more than 250 mm away from the air passage and 50 mm away from APVW-L's inner surface, respectively. So, the suitable distance between two air passages inside APVW-L is 500 mm.

(a) Side view (y=135 mm)

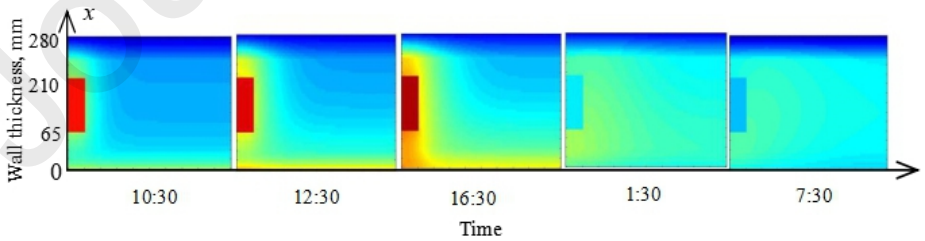

(b) View from the top (z=575 mm)

Note: During the daytime, the air velocity inside vertical air passages is 0.25 m/s; at night, there is no hot air in the air passages, and air velocity is almost 0 m/s.

Fig. 10 Variation in the APVW-L's temperature field with time

5.3.2 Effect of the air velocity inside the vertical air passage

Fig. 11 shows the variation in the APVW-L's heat storage capacity and the GH-20 composite phase change wallboard's phase change rate as air velocity function with the simulated inlet air temperature of 60 ℃. As shown in Fig. 11, GH-20 composite phase change wallboard's maximum heat storage capacity is 1.7 times of that of the cement block/bricks layer, but its thickness is much thinner than cement block/bricks layer's thickness. At night, GH-20 composite phase change wallboard's heat release process is quicker than that of the cement block/bricks layer, and heat storage capacity inside cement block/bricks layer only reduces by 27%. With the increasing of air velocity inside vertical air passage, the increasing trends of heat storage capacity and phase change rate gradually decreases. And the air velocity greater than 0.45 m/s has little influence on the heat storage capacity and phase change rate.

(a) Variation in the heat storage capacity with time **(b) Variation in the phase change rate with time**

Note: P is the GH-20 composite phase change wallboard, and C is the cement block/bricks wall.

Fig. 11 Effect of air velocity on the heat storage capacity and phase change rate

Fig. 12 presents the variation in the heat transfer of the APVW-L's surfaces as functions of the air velocity with the simulated inlet air temperature of 60 ℃. As shown in Fig.12a, the increasing air velocity mainly exerts positive effects on the heat transfer of the APVW-L's inner surface in the afternoon and after midnight. While this increasing trend with the increasing of air velocity becomes more and more obvious with time after midnight. This phenomenon is very important, because the indoor heat load gradually reaches the maximum during this period. But the air velocity greater than 0.45 m/s has little influence on this trend. So the suitable air velocity should be about 0.45 m/s. Fig.12b shows that the positive effects of the heat transfer of the external surface caused by air velocity mainly occur during daytime.

(a) Heat transfer on the inner surface **(b) Heat transfer on the external surface**

Fig. 12 Effect of air velocity on the heat transfer of the APVW-L's surfaces

5.3.3 Effect of inlet air temperature of the vertical air passage

Fig. 13 presents the variation in the APVW-L's heat storage capacity and GH-20 composite phase change wallboard's phase change rate as inlet air temperature function with the simulated the air velocity of 0.45 m/s. As shown in Fig. 13, when inlet air temperature increases, the heat storage capacity and phase change rate increase almost linearly.

(a) Variation of the heat storage capacity with time **(b) Variation of the phase change rate with time**

Note: P is the GH-20 composite phase change wallboard, and C is the cement block/bricks layer.

Fig. 13 Effect of inlet air temperature on the heat storage capacity and phase change rate

Fig. 14 presents the variation in the heat transfer of the APVW-L's surfaces as inlet air temperature function with the simulated the air velocity of 0.45 m/s. As shown in Fig. 14, higher air inlet temperature can effectively improve the heat transfer of the APVW-L's surfaces. As shown in Table 2, on a sunny day, heat loss from external surface accounts for 18.5% of that from the inner surface. So, the thermal insulation performance of the external layer is important for the APVW-L's heat storage performance.

(a) Heat transfer on the inner surface **(b) Heat transfer on the external surface**

Fig. 14 Effect of inlet air temperature on the heat transfer of the APVW-L's surfaces

Table 2 Effects of inlet air temperature and air velocity on the heat transfer of the APVW-L's surfaces throughout the day

Inlet air temperature, ℃		60				40	50	60	70
Air velocity, m/s		0.25	0.35	0.45	0.55	0.45			
Heat transfer, MJ/m^2	Inner surface	8.2	8.5	8.6	8.7	8.1	8.34	8.6	8.7
	External surface	1.6	1.6	1.7	1.7	1.5	1.6	1.7	1.7

5.3.4 Effect of the thickness of each material layer inside the APVW-L

The control variable method was taken for quantitatively analyzing the effect of insulation layer's thickness and GH-20 composite phase change wallboard's thickness on the APVW-L's thermal performance. See Table 3, the numerical cases are Case1 and Case 2 respectively.

Table 3 Conditional assumptions

Case	Inlet air temperature, ℃	Air velocity, m/s	Thickness of phase change layer, m	Thickness of insulation layer, m
Case1	60	0.45	0.04	0.06~0.18
Case2	60	0.45	0.03~0.05	0.15

Fig. 15 shows the effect of insulation layer's thickness on the APVW-L's thermal performance (Case 1). As shown in Fig. 15a, the increasing of insulation layer's thickness affects the cement block/bricks layer's heat storage capacity, but this effect is weakened gradually with the increasing of insulation layer's thickness. As shown in Fig. 15b, as insulation layer's thickness increases, heat loss from external surface gradually decreases, and this tend to be stable after 0.14 m. Therefore, when the APVW-L is applied in Beijing, the insulation layer's thickness should not be less than 0.14 m.

(a) Variation in cement block/bricks layer's heat storage capacity with time

(b) Variation in heat loss from the external surface with insulation layer's thickness

Fig. 15 Effect of insulation layer's thickness on APVW-L's thermal performance (Case 1)

Fig. 16 shows the effect of phase change material layer's thickness on the APVW-L's thermal performance (Case 2). For each 0.01 m increase in the phase change material layer's thickness, phase change material layer's heat storage capacity

increases, but cement block/bricks layer's maximum heat storage capacity, phase change material layer's maximum phase change rate and the change after midnight of cement block/bricks layer's heat storage capacity decrease. Accordingly, a very thick PCM layer is neither conducive to this wall for absorbing solar energy during daytime nor to releasing the heat inside the wall to the room at night. So phase change material layer's proper thickness should be 0.04 m when the APVW-L is applied in Beijing.

(a) Variation in the heat storage capacity with time **(b) Variation in the phase change rate with time**

Note: P is GH-20 composite phase change wallboard, and C is cement block/bricks layer.

Fig. 16 Effect of the PCM layer's thickness on APVW-L's thermal performance (Case 2)

In conclusion, the optimized APVW-L could store 5.63 MJ/(m^2·day) of solar energy in an active-passive way in Beijing, and phase change material layer's phase change rate was 77.7%. After the whole night, the heat storage capacity of phase change material layer and cement block/bricks layer decreased by 86% and 21% respectively.

6. Experimental analysis of APVW-L in the solar greenhouse

After optimization as described in Section 5, a full-scale and optimized APVW-L equipped with solar air collector system was integrated into the back-wall of an experimental greenhouse in Beijing. Fig.17 shows the appearance of the system with APVW-L in the experimental greenhouse. Except for the back-wall, the structural dimensions, materials and test procedures of this experimental greenhouse were identical to those of the conventional greenhouse. The solar air collector system ran from 8:30 to 16:30 on sunny days. The APVW-L's air velocity was set according to the design air velocity of 0.45 m/s proposed in Section 5.3.2. The experimental tests and data acquisition methods are consistent with [34].

Fig. 17 Appearance of the APVW-L integrated into a solar greenhouse's back-wall

The APVW-L's mathematical model proposed in Section 3 can be used for predicting its thermal performance in practical projects. Fig. 18 presents the simulated and measured values of the APVW-L's surface temperatures and vertical air passage's outlet air temperature between December 19, 2019 to December 22, 2019. Compared to [32], the average absolute error and maximum absolute error of the proposed model in predicting the APVW-L's inner surface temperatures were smaller. This model also verified the APVW-L's external surface temperature and vertical air passage's outlet air temperature against the experimental results, and exhibited a high accuracy. As shown in Table 4, The *IA*, *NMBE* and *RMSE* were 1.74%~5.81%, 1.40%~3.20% and 0.992~0.996, respectively. Combined with the analyses in section 4.3, the proposed model could dynamically predict the APVW-L's thermal performance under changeable meteorological conditions.

(a) Internal surface temperature **(b) External surface temperature**

(c) Outlet air temperature

Fig. 18 Simulated and measured values of the APVW-L in an experimental greenhouse

Table 4 Error analysis of numerical calculation

Index	Mean absolute error, ℃	Maximum absolute error, ℃	*IA*	*NMBE*, %	*RMSE*, %
Interior	0.85	2.98	0.	5.81	1.4

surface			996		0
Outer surface	1.07	3.29	0.992	4.77	2.28
Outlet air	0.45	1.90	0.993	1.74	3.20

Fig. 19 shows the experimental values in the experimental greenhouse and the conventional greenhouse. These values were obtained during the period between 23 January, 2020 and 19 February, 2020, when it was the coldest in Beijing. The experimental results demonstrated that the indoor air temperature reached the lowest level after midnight. The APVW-L promoted the back-wall's average interior surface by 2.2~3.4 ℃ and average indoor air temperature by 0.8~1.4 ℃ after midnight. February 14, 2020 was a cloudy and snowy day (the 23rd day in Fig. 19) and the outdoor solar radiation in the daytime was not enough for operating the MSC-DRTs. On that day, the system still increased the back-wall's average interior surface by 2.2 ℃ and average indoor air temperature by 0.8 ℃ after midnight.

(a) Back-wall's interior surface temperature **(b) Indoor air temperature**

Fig. 19 Application outcome of the APVW-L in the solar greenhouse in winter

7. Conclusions

1. A proposed design of an APVW-L, measured in a laboratory prototype, was integrated into a solar greenhouse by deploying a full-scale prototype. And an APVW-L's mathematical model was proposed and well-validated against the measured data from both laboratory and full-scale prototypes.

2. When using APVW-L in Beijing, the PCM layer's thickness should be 0.04 m, the insulation layer's thickness should not be less than 0.14 m, the suitable distance between two air passages should be 500 mm, and the suitable air velocity inside vertical air passage should be 0.45 m/s.

3. On a sunny day in Beijing, APVW-L could store 5.36 MJ/(m^2·day) of solar energy in an active-passive way. After the whole night, the heat storage capacity of PCM layer

and cement block/bricks layer decreased by 86% and 21% respectively.

4. In comparison to the conventional greenhouse, the experimental greenhouse using APVW-L increased the back-wall's average interior surface by 2.2~3.4 ℃ and average indoor air temperature by 0.8~1.4 ℃ after midnight.

Acknowledgement

The program was sponsored by the National Natural Science Foundation of China (51368060, 51578012); Key R & D projects of Ningxia Hui Autonomous Region (2019BFF02005); National Key R & D Program of the "13th Five Year Plan" Period (2016YFC0700206).

Reference

1. Bao E., Cao Y., Zou Z., et al., Research progress of thermal storage technology in energy-saving solar greenhouse, Transactions of the Chinese Society of Agricultural Engineering (Transactions of the CSAE) 34(6) (2018) 1-14.

2. N. Zhou, Y. Yu, J. Yi, et al., A study on thermal calculation method for a plastic greenhouse with solar energy storage and heating, Solar Energy 142 (2017) 39-48.

3. G. M. Hassan, A. Yahya, F. R. Seyed, et al., Solar energy conservation in greenhouse: thermal analysis and experimental validation, Renewable Energy 96 (2016) 509-519.

4. Sethi V., Sharma S., Survey and evaluation of heating technologies for worldwide agricultural greenhouse applications, Solar Energy, 82 (9) (2008) 832-859.

5. Wei B., Guo S. R., Wang J., et al., Thermal performance of single span greenhouses with removable back walls, Biosystems Engineering 141 (2016) 48-57.

6. F. Berroug, E. K. Lakhal, M. EI Omari, et al., Thermal performance of a greenhouse with a phase change material north wall, Energy and Buildings 43(11) (2011) 3027-3035.

7. C. Chen, H. S. Ling, Z. Q. Zhai, et al., Thermal performance of an active-passive ventilation wall with phase change material in solar greenhouses, Applied Energy 216 (2018) 602–612.

8. Y. Guan, C. Chen, Y. Han, et al., Experimental and modeling analysis of a three-layer wall with phase-change thermal storage in a Chinese solar greenhouse, Journal of Building Physics 38 (6) (2015) 548–559.

9. Yong Guan, Tuo Wang, Rui Tang, et al., Numerical study on the heat release capacity of the active-passive phase change wall affected by ventilation velocity, Renewable Energy 150 (2020) 1047–1056.

10. Fang H, Yang Q, Zhang Y, et al., Performance of a solar heat collection and release system for improving night temperature in a Chinese solar greenhouse, Applied

Engineering in Agriculture 31 (2) (2015) 283–289.

11. Elghamry R., Hassan H., Impact of window parameters on the building envelope on the thermal comfort, energy consumption and cost and environment, International Journal of Ventilation 19 (4) (2019a) 233–259.

12. Cole R. J., Fedoruk L., Shifting from net-zero to net-positive energy buildings, Building research and information 43 (2015) 111–120.

13. Rania Elghamry, Hamdy Hassan, Experimental investigation of building heating anventilation by using Trombe wall coupled with renewable energy system under semi-arid climate conditions, Solar Energy 201 (2020) 63–74.

14. Hassanain A. A., Hokam E. M., Mallick T. K., Effect of solar storage wall on the passive solar heating constructions, Energy and Buildings, 43 (2-3) (2010) 737–747.

15. E. Bao, T. Shen, Y. Zhang, et al., Thermal performance analysis of assembled active heat storage wall in Chinese solar greenhouse. Transactions of the Chinese Society of Agricultural Engineering (Transactions of the CSAE) 34 (10) (2018) 178–186.

16. E. Bao, Y. Cao, Z. Zou, Y. Zhang, Characteristic of heat transfer for active heat storage wall with different structures in Chinese solar greenhouse, Transactions of the Chinese Society of Agricultural Engineering (Transactions of the CSAE) 35(3) (2019) 189–197.

17. Sethi V., Sharma S., Survey and evaluation of heating technologies for worldwide agricultural greenhouse applications, Solar Energy 82 (9) (2008) 832–859.

18. Zhang X., Wang H. L., Zou Z. R., et al., CFD and weighted entropy based simulation and optimisation of Chinese Solar Greenhouse temperature distribution, Biosystems Engineering 142 (2016) 12–26.

19. Yataganbaba A., Ozkahraman B., Kurtbas I., Worldwide trends on encapsulation of phase change materials: a bibliometric analysis (1990–2015), Applied Energy 185 (2017) 720–731.

20. Chao C., Nan Y., Fengguang Y. et al., Theoretical and experimental study on selection of physical dimensions of passive solar greenhouses for enhanced energy performance, Solar Energy, 191 (2019) 46–56.

21. K. K. Roman, T. O'Brien, J. B. Alvey, et al., Simulating the effects of cool roof and PCM (phase change materials) based roof to mitigate UHI (urban heat island) in prominent US cities, Energy 96 (2016) 103–117.

22. Ma Q., Fukuda H., Wei X., et al., Optimizing energy performance of a ventilated composite Trombe wall in an office building, Renewable Energy 134 (2019) 1285–1294.

23. Y. Q. Nguyen, J. C. Wells, A numerical study on induced flowrate and thermal efficiency of a solar chimney with horizontal absorber surface for ventilation of buildings, Journal of Building Engineering, 28 (2020) 101050.

24. Tong Guohong, David M. Christopher, Temperature variations in energy storage layers in Chinese solar greenhouse walls, Transactions of the Chinese Society of Agricultural Engineering (Transactions of the CSAE) 35 (7) (2019) 170–177.

25. Bao Encai, Zou Zhirong, Zhang Yong, CFD simulation of heat transfer in back-wall of active thermal-storage solar greenhouse with different airflow directions, Transactions of the Chinese Society of Agricultural Engineering (Transactions of the CSAE) 34 (22) (2018) 169–177.

26. Jovanovic J., Sun X., Stevovic S., et al., Energy-efficiency gain by combination of PV modules and Trombe wall in the low-energy building design, Energy and Buildings 152 (2017) 568–576.

27. Lin Y., Ji J., Lu X., et al, Thermal and electrical behavior of built-middle photovoltaic integrated Trombe wall: Experimental and numerical study, Energy 189 (2019a) 116173.

28. Lin Y., Ji J., Zhou F., et al., Experimental and numerical study on the performance of a built-middle PV Trombe wall system, Energy and Buildings 200 (2019b) 47–57.

29. Zhang X, Wang H, Zou Z, et al., CFD and weighted entropy based simulation and optimisation of Chinese Solar greenhouse temperature distribution, Biosystems Engineering 142 (2016) 12–26.

30. Zhang Qunli, Gao Yan, Di Hongfa, Research on thermal performance characteristics of ideal passive building with phase change material for thermal storage, Acta Energiae Solaris Sinica 36 (8) (2015) 2021–2027

31. Shuqin Chen, Yipan Zhu, Yue Chen, et al., Usage strategy of phase change materials in plastic greenhouses, in hot summer and cold winter climate, Applied Energy 277 (2020) 115416.

32. Haoshu Ling, Liang Wanga, Chao Chen, et al., Effect of thermophysical properties correlation of phase change material on numerical modelling of agricultural building, Applied Thermal Engineering 157 (2019) 113579.

33. S. N. AL-Saadi, Z. Q. Zhai, Modeling phase change materials embedded in building enclosure: a review, Renew. Sustain. Energy Rev. 21 (2013) 659–673.

34. Chao Chen, Fengtao Han, Khamid Mahkamov, et al., Numerical and experimental study of laboratory and full-scale prototypes of the novel solar multi-surface air collector with double-receiver tubes integrated into a greenhouse heating system, Solar Energy 202 (2020) 86–103.

35. Chen Chao, Ling Haoshu, Yu Nan, et al., Calculation method of heat storage coefficient of phase change material, Acta Energiae solaris Sinica 39(2018): 2267-2272.

36. Ling H, Chen C, Guan Y, et al, Active heat storage characteristics of active-passive triple wall with phase change material, Solar Energy 110 (2014) 276–285.

37. Zhang Ximin, Ren Zepei, Mei Feiming et al., Heat Transfer, China Architecture & Building Press, Beijing (China), 2007 341p ISBN 978-7-112-09183-6.

38. Fu Xiangzhao, Xiao Yimin., Fluid network for transportation and distribution, China Architecture & Building Press, Beijing (China), 2010, 337p, ISBN 978-7-112 -11550-1.

39. Guohong Tong, David M. Christopher, Guoqing Zhang, New insights on span selection for Chinese solar greenhouse using CFD analysis, Computers and Electronics in Agriculture 149 (2018) 3-15.

40. Watmuff, J. H., Charters, W. W. S., Proctor, D., Solar and wind induced external coefficients for solar collectors, Revue Internationale D'Heliotechnique 2 (1977) 56.

41. ASHRAE guideline: measurement of energy and demand savings, American Society of Heating R, Air-Conditioning E, Atlanta, 2012.

42. Nan Yu, Chao Chen, Khamid Mahkamov, et al., Selection of a phase change material and its thickness for application in walls of buildings for solar-assisted steam curing of precast concrete, Renewable Energy 150 (2020) 808-820.

Author Statement

This study has developed a mathematical model for an active-passive ventilation wall with latent heat storage, and this model was well-validated against the measured data from both laboratory and full-scale prototypes. Using this model, the optimization design and operation strategy of the APVW-L in the solar greenhouse could be obtained. This study demonstrated that the optimized APVW-L could store 5.36 MJ/(m2·day) of solar energy in Beijing. Compared to the identical conventional greenhouses, after midnight, the experimental greenhouse having APVW-L increased the back-wall's interior surface temperature by 2.2~3.4 °C, and the average indoor air temperature by 0.8~1.4 °C. This study provides methods for the APVW-L's optimization design and its operation strategy, even for the rationalization of the near-zero energy consumption of the solar greenhouse during winter.

The corresponding author of this Manuscript is Chao Chen. All authors read and contributed to the manuscript.

Prof. Chao Chen
Beijing Key Laboratory of Green Building Environment and Energy-Efficiency Technology,
Beijing University of Technology,
Beijing 100124, P R China.
Tel：86-010-67391608-201
Email: chenchao@bjut.edu.cn

Conflict of Interest

The manuscript has not been published previously by any of the authors and/or is not under consideration for publication in another journal at the time of submission. And all authors in this work have no question about conflict of interest including any financial, personal or other relationships with other people or organizations within three years of beginning the submitted work.